

Two families of non-local scattering models and the weighted curvature

Tanos Elfouhaily[†], Christophe Bourlier[‡], and Joel T. Johnson[§]

[†] Centre National de la Recherche Scientifique, IRPHE, Marseille, France

[‡] IREENA, Ecole polytechnique de l'université de Nantes, Nantes, France

[§] Dept of Electrical Engineering, The Ohio State University, Columbus, OH USA

Abstract. There are several nonlocal scattering models available in the literature. Most of them are given with little or no mention of their expected accuracy. Moreover, high and low frequency limits are rarely tested. The most important limits are the low-frequency or the small perturbation method (SPM) and the high-frequency Kirchhoff approximation (KA) or the geometric optics (GO). We are interested in providing some insight into two families of nonlocal scattering models. The first family of models is based on the Meecham-Lysanov Ansatz (MLA). This ansatz includes the nonlocal small slope approximation (NLSSA) by Voronovich and the operator expansion method by Milder (OEM). A quick review of this first family of models is given along with a novel derivation of a series of kernels which extend the existing models to include some more fundamental properties and limits. The second family is derived from formal iterations of geometric optics which we call the Ray Tracing Ansatz (RTA). For this family we consider two possible kernels. The first is obtained from iteration of the high-frequency Kirchhoff approximation, while the second is an iteration of the weighted curvature approximation. In the latter case we find that most of the required limits and fundamental conditions are fulfilled, including tilt invariance and reciprocity. A study of scattering from Dirichlet sinusoidal gratings is then provided to further illustrate the performance of the models considered.

PACS numbers: 42.25.Fx, 92.10.Hm, 92.10.Cg

1. Introduction

Scattering of electromagnetic or acoustic waves from rough surface is an interesting problem due to its wide applications in current physics projects, including remote sensing. Current scattering theories are based mostly on development of a smallness parameter. For the most part the accuracy of these models is not well established.

We will analyze two families of multiple scattering models. The first can be classified under the Meecham-Lysanov Ansatz (MLA). This family includes the Meecham-Lysanov Model (MLM) [1, 2, 3], the nonlocal small slope approximation (NLSSA) by Voronovich [4], and the operator expansion method (OEM) by Milder [5], and more recently the nonlocal curvature approximation (NLCA) by Elfouhaily et al.[6] and the phase factor representation PFR by Tatartskii [7]. The second family can be based on what we call the ray tracing ansatz (RTA)(i.e., Garcia et al. [8], Jin and Lax [9], and Macaskill [10]). This family encompasses all models based on the iterations of the Kirchhoff model among them we cite the extended Kirchhoff approximation by Ishimaru [11] and the integral equation method (IEM) by Fung [12, 13].

There are some mandatory limits that any scattering model must reproduce in order to qualify for a wide range of applications over different rough surfaces especially those which include multiple scales. We identify two fundamental limits, the small perturbation method (SPM) and the high-frequency Kirchhoff (KA) or geometric optics (GO). It must be noted that these two limits can be of first or second order depending on whether local or nonlocal effects are considered. It is therefore interesting to have a local model which complies with the SPM-1 and GO-1 limits while its nonlocal extension includes SPM-2 and GO-2 limits, if possible. Unfortunately, in the literature one can find a plethora of scattering models were some of the mentioned limits are not reached regardless of whether the model is local or nonlocal. Most models are in fact not even checked to reveal their compliance with these compulsory limits. A specific example is the original IEM [12], which was used for more than 10 years even though it did not reproduce the SPM-1 limit under general bistatic conditions (see, [14]). This deficiency was later corrected by Alvarez-Perez [13] and adopted by Fung and his co-authors [15].

In this paper we analyze properties of nonlocal models based on either the MLA (such as NLSSA) or the RTA (such as IEM). We begin by identifying a deficiency in NLSSA with regard to the first and second order geometric optics (GO-1 and GO-2) limits. We show that a modified kernel NLSSA can be derived that obtains the GO-1 limit. However the GO-2 limit is found not reachable by NLSSA regardless of the kernel used since the deficiency is identified in the ansatz itself.

We then consider the RTA, and show that for Neumann, Dirichlet, and perfect conducting boundary conditions, a simple nonlocal model can be found by imposing formal compliance with the high-frequency GO-1 and GO-2. It is also shown that by accident SPM-1 is reached under the low-frequency limit. However generalization of this model to the general dielectric case is not found to be easily possible. To address this issue, an iterative weighted curvature approximation (WCA) based on the RTA is

proposed. The local WCA method was recently developed by Elfouhaily et al. [6], and achieves both the GO-1 and SPM-1 limits in the dielectric case while retaining a form as simple as the tangent plane approximation. The iterative WCA developed retains the GO-1 and SPM-1 limits of the local model while the iterative procedure of the RTA ensures compliance with the GO-2 limit. A study of the performance of both existing and newly developed local and non-local models is then presented in terms of scattering from a one-dimensional sinusoidal grating for the Dirichlet case. Results confirm the analytical performances expected, although the choice of a particular model for the greatest accuracy remains dependent on the surface of interest.

2. The Meecham-Lysanov Ansatz

The Meecham-Lysanov model (MLM) [1, 2] was developed for acoustic scattering under Dirichlet boundary conditions. Its nonlocal ansatz survived extensions to more general boundary conditions such as those by the nonlocal small slope approximation (NLSSA) by Voronovich [4] and the operation extension method (OEM) by Milder [5, 16]. For simplicity we reveal these details through the notation and form of NLSSA.

2.1. Formulation

In a follow up on the local small slope approximation in [17], Voronovich generalized his model to include non-local scattering mechanisms such as double reflection on the surface. The ansatz used by Voronovich in [4] conforms to the Meecham-Lysanov ansatz (MLA) and has the explicit expression

$$\mathcal{S}(\mathbf{k}, \mathbf{k}_0) = \iiint \phi(\mathbf{k}, \mathbf{k}_0; \boldsymbol{\xi}) e^{-i(\mathbf{k}-\boldsymbol{\xi}) \cdot \mathbf{x}_1 - iq_k \eta(\mathbf{x}_1)} e^{i(\mathbf{k}_0-\boldsymbol{\xi}) \cdot \mathbf{x}_2 - iq_0 \eta(\mathbf{x}_2)} d\boldsymbol{\xi} d\mathbf{x}_1 d\mathbf{x}_2 \quad (1)$$

where $\phi(\mathbf{k}, \mathbf{k}_0; \boldsymbol{\xi})$ is the non-local kernel, $\eta(\mathbf{x})$ is a rough surface (which could be random as well), and the incident \mathbf{K}_i and scattered \mathbf{K}_s wavenumbers are defined as

$$\mathbf{K}_i = \mathbf{k}_0 - q_0 \hat{z} \quad (2a)$$

$$\mathbf{K}_s = \mathbf{k} + q_k \hat{z} \quad (2b)$$

$$q_{\boldsymbol{\xi}} = \sqrt{K^2 - \boldsymbol{\xi} \cdot \boldsymbol{\xi}} \quad (2c)$$

$$|\mathbf{K}_i| = |\mathbf{K}_s| = K \quad (2d)$$

If the kernel function ϕ is chosen to satisfy

$$\phi(\mathbf{k}, \mathbf{k}_0; \boldsymbol{\xi}) = \phi^T(-\mathbf{k}_0, -\mathbf{k}; -\boldsymbol{\xi}) \quad (3)$$

then the MLA satisfies the fundamental properties of reciprocity as well as vertical and horizontal shift invariance:

$$\mathcal{S}(\mathbf{k}, \mathbf{k}_0) = \mathcal{S}^T(-\mathbf{k}_0, -\mathbf{k}) \quad (4a)$$

$$\mathcal{S}(\mathbf{k}, \mathbf{k}_0) \Big|_{\eta+H} = e^{-iQ_z H} \mathcal{S}(\mathbf{k}, \mathbf{k}_0) \Big|_{\eta} \quad (4b)$$

$$\mathcal{S}(\mathbf{k}, \mathbf{k}_0) \Big|_{\eta(\mathbf{x}-\mathbf{d})} = e^{-iQ_H \cdot \mathbf{d}} \mathcal{S}(\mathbf{k}, \mathbf{k}_0) \Big|_{\eta} \quad (4c)$$

where

$$Q_z = q_0 + q_k \quad (5a)$$

$$\mathbf{Q}_H = \mathbf{k} - \mathbf{k}_0 \quad (5b)$$

Voronovich in [4] suggested a derivation of the kernel $\phi(\mathbf{k}, \mathbf{k}_0; \boldsymbol{\xi})$ based on matching both the first and second order small perturbation methods (SPM-1 and SPM-2). The resulting kernel function is

$$\phi(\mathbf{k}, \mathbf{k}_0; \boldsymbol{\xi}) = \frac{\mathcal{B}(\mathbf{k}, \mathbf{k}_0)}{Q_z} + \frac{\mathcal{B}_2(\mathbf{k}, \mathbf{k}_0; \boldsymbol{\xi}) - \mathcal{B}_2(\mathbf{k}, \mathbf{k}_0; \mathbf{k}_0)}{q_0} + \frac{\mathcal{B}_2(\mathbf{k}, \mathbf{k}_0; \boldsymbol{\xi}) - \mathcal{B}_2(\mathbf{k}, \mathbf{k}_0; \mathbf{k})}{q_k} \quad (6)$$

where B and B_2 refer to the SPM kernel functions shown in the appendix of this paper. This kernel will be referred to as the NLSSA kernel throughout the remainder of the paper. However, use of the NLSSA kernel in the MLA does not guarantee convergence toward the GO-1 or GO-2 limits, as will be examined in the next section.

2.2. First order geometric optics from MLA

The high-frequency limit of the NLSSA ansatz as in (1) can be derived by invoking the stationary phase theorem and single reflection, hence

$$\mathcal{S}(\mathbf{k}, \mathbf{k}_0) = \phi(\mathbf{k}, \mathbf{k}_0; \boldsymbol{\xi}_s) \int e^{-iQ_z \eta(\mathbf{x})} e^{-i\mathbf{Q}_H \cdot \mathbf{x}} d\mathbf{x} \quad (7)$$

where the originally dummy integration variable $\boldsymbol{\xi}$ is now evaluated at the stationary point:

$$\boldsymbol{\xi}_s = \frac{q_k \mathbf{k}_0 + q_0 \mathbf{k}}{q_k + q_0} \quad (8)$$

In order for NLSSA to be able to reproduce the first order geometric optics limit (GO-1), the following condition must be satisfied

$$\frac{\mathcal{K}}{Q_z} = \phi\left(\mathbf{k}, \mathbf{k}_0; \frac{q_k \mathbf{k}_0 + q_0 \mathbf{k}}{q_k + q_0}\right) \quad (9)$$

where \mathcal{K} is the polarization matrix of the high-frequency Kirchhoff in the notation of [6]. Satisfying the GO-1 condition in (9) formally is nearly impossible (unless it is used originally to define ϕ). For this reason, one can use the following identities

$$\boldsymbol{\xi}_s = \frac{q_k \mathbf{k}_0 + q_0 \mathbf{k}}{q_k + q_0} = \mathbf{k} - q_k \frac{\mathbf{Q}_H}{Q_z} = \mathbf{k}_0 + q_0 \frac{\mathbf{Q}_H}{Q_z} \quad (10)$$

along with a Taylor expansion of (9) in powers of \mathbf{Q}_H . In this case, one can satisfy the GO-1 condition only approximately up to some order in \mathbf{Q}_H .

$$\frac{\mathcal{K}}{Q_z} = \frac{1}{2} \left\{ \phi(\mathbf{k}, \mathbf{k}_0; \mathbf{k} - q_k \frac{\mathbf{Q}_H}{Q_z}) + \phi(\mathbf{k}, \mathbf{k}_0; \mathbf{k}_0 + q_0 \frac{\mathbf{Q}_H}{Q_z}) \right\} \quad (11)$$

$$\approx \frac{1}{2} \left\{ \phi(\mathbf{k}, \mathbf{k}_0; \mathbf{k}) + \phi(\mathbf{k}, \mathbf{k}_0; \mathbf{k}_0) \right. \quad (12)$$

$$\left. - [q_k \nabla \phi(\mathbf{k}, \mathbf{k}_0; \mathbf{k}) - q_0 \nabla \phi(\mathbf{k}, \mathbf{k}_0; \mathbf{k}_0)] \cdot \frac{\mathbf{Q}_H}{Q_z} \right.$$

$$\left. + \frac{1}{2} \frac{\mathbf{Q}_H}{Q_z} \cdot [q_k^2 \nabla \nabla \phi(\mathbf{k}, \mathbf{k}_0; \mathbf{k}) + q_0^2 \nabla \nabla \phi(\mathbf{k}, \mathbf{k}_0; \mathbf{k}_0)] \cdot \frac{\mathbf{Q}_H}{Q_z} + \dots \right\}$$

Using equation (6) and the identities in the appendix, it is straight forward to show that the NLSSA does not satisfy this condition in the quadratic order for the Dirichlet, Neumann, or perfect conducting boundary conditions, contrary to equation 5.3 in [4]. The original local SSA [3] does not reach GO-1 for the dielectric case only. It is therefore clear that enforcing the SPM-1 and SPM-2 limits in the MLA does not guarantee the GO-1 limit even for perfect conducting boundary conditions.

2.3. Modified non-local kernels

Different kernels can be proposed for the MLA to attempt to reach both the SPM-1 and high frequency limits. Such kernels can be based on the SPM-2 but without necessarily reproducing the SPM-2 limit. Using the identities of the appendix, we can derive a new kernel as

$$\phi(\mathbf{k}, \mathbf{k}_0; \boldsymbol{\xi}) = \frac{q_k + q_0}{2q_k q_0} \mathcal{B}_2(\mathbf{k}, \mathbf{k}_0; \boldsymbol{\xi}) \quad (13)$$

This result can be considered as a simplification of the first order operator expansion method (OEM) developed by Milder [5, 18] and a generalization of the Meecham-Lysanov model [1, 2]; the kernel will be referred to as the Meecham-Lysanov model (MLM) kernel throughout the remainder of the paper. Equation (13) is simple because it is readily applicable to Neumann, Dirichlet, perfect conduction, dielectric boundary conditions, indifferently. Using the identities of the appendix, it can be demonstrated that this kernel satisfies both the SPM-1 and GO-1 limits for Neumann, Dirichlet, and perfect conducting surfaces, but not the SPM-2 limit. It can also be shown that this scattering model is not tilt invariant; for a definition of tilt invariance the reader is referred to [6, 19].

It is possible to enforce in addition to SPM-1 and GO-1, the SPM-2 limit through a relation similar to equation 18 in [6],

$$\phi(\mathbf{k}, \mathbf{k}_0; \boldsymbol{\xi}) = \alpha + \beta \mathcal{B}_2(\mathbf{k}, \mathbf{k}_0; \boldsymbol{\xi}) + \gamma \mathcal{B}_2(\mathbf{k}, \mathbf{k}_0; \mathbf{k} + \mathbf{k}_0 - \boldsymbol{\xi}), \quad (14)$$

where α , β , and γ three constants to be determined by imposing three relevant conditions. If γ is set to zero and a solution is sought for α and β from imposing the SPM-1 and SPM-2 limits, one gets the NLSSA. If however one imposes in addition to SPM-1 and SPM-2, the high frequency GO-1 limit for Neumann, Dirichlet, and perfectly-conducting surfaces, the constant γ becomes necessary as another degree of freedom. After some tedious algebraic manipulations, one finds

$$\phi(\mathbf{k}, \mathbf{k}_0; \boldsymbol{\xi}) = \frac{q_k + q_0}{2q_k q_0} \left[\mathcal{B}_2(\mathbf{k}, \mathbf{k}_0; \boldsymbol{\xi}) + \mathcal{B}_2(\mathbf{k}, \mathbf{k}_0; \mathbf{k} + \mathbf{k}_0 - \boldsymbol{\xi}) - \frac{q_k^2 + q_0^2}{(q_k + q_0)^2} \mathcal{B}(\mathbf{k}, \mathbf{k}_0) \right] \quad (15)$$

or equivalently,

$$\phi(\mathbf{k}, \mathbf{k}_0; \boldsymbol{\xi}) = \frac{\mathcal{B}(\mathbf{k}, \mathbf{k}_0)}{Q_z} + \frac{q_k + q_0}{2q_k q_0} [\mathcal{B}_2(\mathbf{k}, \mathbf{k}_0; \boldsymbol{\xi}) + \mathcal{B}_2(\mathbf{k}, \mathbf{k}_0; \mathbf{k} + \mathbf{k}_0 - \boldsymbol{\xi}) - \mathcal{B}(\mathbf{k}, \mathbf{k}_0)] \quad (16)$$

As with the NLSSA, the latest form separates the local SSA-1 contribution (first term) from the nonlocal correction. This kernel function will be referred to as the modified

non-local SSA (MNLSSA) kernel in the remainder of the paper. It can be shown that the MNLSSA kernel produces a tilt invariant theory when used in the MLA. This non-local kernel in (16) is therefore analytically highly appropriate but unfortunately still does not reach the second-order high-frequency Kirchhoff as explained in what follows.

2.4. Second order geometric optics from MLA

We perform a comparison of the MLA with the GO-2 limit in the incoherent ensemble average case where the second order geometric optics is known to have the form (see equation 51a [20] or equation 51 [13]):

$$\langle \mathcal{S}(\mathbf{k}, \mathbf{k}_0) \mathcal{S}^*(\mathbf{k}, \mathbf{k}_0) \rangle = \int \left| \frac{\phi(\mathbf{k}, \mathbf{k}_0; \boldsymbol{\xi}) - \phi(\mathbf{k}, \mathbf{k}_0; \boldsymbol{\xi}_s)}{(q_k \pm q_{\boldsymbol{\xi}})(q_0 \mp q_{\boldsymbol{\xi}})} \right|^2 P \left(-\frac{\mathbf{k} - \boldsymbol{\xi}}{q_k \pm q_{\boldsymbol{\xi}}}, \frac{\mathbf{k}_0 - \boldsymbol{\xi}}{q_0 \mp q_{\boldsymbol{\xi}}} \right) d\boldsymbol{\xi} \quad (17)$$

where P is the joint probability density function (pdf) of the slopes at two different locations on the surface, and ϕ is a kernel associated with the GO-2 model. The above equation can be interpreted by considering a scattering process in which the incident wave is specularly scattered into the $\boldsymbol{\xi}$ direction, when is then specularly re-scattered into the observation direction. Consideration of the slopes required for this process results in the arguments observed in the slope probability density function above; these arguments are similar to those observed in single point slope pdf for the local GO-1 model. The integration adds the contributions from all possible directions of the intermediate wave $\boldsymbol{\xi}$ (note $\boldsymbol{\xi}$ is the horizontal projection of the propagation direction). The plus-and-minus signs in this expression account for the possibility of the intermediate waves propagating either upward or downward.

Now compute the ensemble average of the modulus of the scattering matrix in (1)

$$\begin{aligned} \langle \mathcal{S}(\mathbf{k}, \mathbf{k}_0) \mathcal{S}^*(\mathbf{k}, \mathbf{k}_0) \rangle &= \iiint \iiint \phi(\mathbf{k}, \mathbf{k}_0; \boldsymbol{\xi}_1) \phi^*(\mathbf{k}, \mathbf{k}_0; \boldsymbol{\xi}_2) \\ &\quad \langle e^{-i(\mathbf{k}-\boldsymbol{\xi}_1) \cdot \mathbf{x}_1 - iq_k \eta_1} e^{i(\mathbf{k}_0-\boldsymbol{\xi}_1) \cdot \mathbf{x}_2 - iq_0 \eta_2} \\ &\quad e^{i(\mathbf{k}-\boldsymbol{\xi}_2) \cdot \mathbf{x}_3 + iq_k \eta_3} e^{-i(\mathbf{k}_0-\boldsymbol{\xi}_2) \cdot \mathbf{x}_4 + iq_0 \eta_4} \rangle \\ &\quad d\boldsymbol{\xi}_1 d\boldsymbol{\xi}_2 d\mathbf{x}_1 d\mathbf{x}_2 d\mathbf{x}_3 d\mathbf{x}_4 \end{aligned} \quad (18)$$

After expansion in the phase of the difference of elevations in the slope times the difference of positions, we rewrite (18) as

$$\begin{aligned} \langle \mathcal{S}(\mathbf{k}, \mathbf{k}_0) \mathcal{S}^*(\mathbf{k}, \mathbf{k}_0) \rangle &= \iiint \iiint \phi(\mathbf{k}, \mathbf{k}_0; \boldsymbol{\xi}_1) \phi^*(\mathbf{k}, \mathbf{k}_0; \boldsymbol{\xi}_2) P(\nabla \eta_1, \nabla \eta_2) \\ &\quad e^{-iq_k \nabla \eta_1 (\mathbf{x}_1 - \mathbf{x}_3) - iq_0 \nabla \eta_2 (\mathbf{x}_2 - \mathbf{x}_4)} \\ &\quad e^{-i(\mathbf{k}-\boldsymbol{\xi}_1) \cdot \mathbf{x}_1 + i(\mathbf{k}_0-\boldsymbol{\xi}_1) \cdot \mathbf{x}_2} \\ &\quad e^{i(\mathbf{k}-\boldsymbol{\xi}_2) \cdot \mathbf{x}_3 - i(\mathbf{k}_0-\boldsymbol{\xi}_2) \cdot \mathbf{x}_4} \\ &\quad d\boldsymbol{\xi}_1 d\boldsymbol{\xi}_2 d\mathbf{x}_1 d\mathbf{x}_2 d\mathbf{x}_3 d\mathbf{x}_4 d\nabla \eta_1 d\nabla \eta_2 \end{aligned} \quad (19)$$

We then find, after a change of variables to sum and differences coordinates and using the stationary phase approximation:

$$\langle \mathcal{S}(\mathbf{k}, \mathbf{k}_0) \mathcal{S}^*(\mathbf{k}, \mathbf{k}_0) \rangle = \int \left| \frac{\phi(\mathbf{k}, \mathbf{k}_0; \boldsymbol{\xi}) - \phi(\mathbf{k}, \mathbf{k}_0; \boldsymbol{\xi}_s)}{q_0 q_k} \right|^2 P \left(-\frac{\mathbf{k} - \boldsymbol{\xi}}{q_k}, -\frac{\boldsymbol{\xi} - \mathbf{k}_0}{q_0} \right) d\boldsymbol{\xi} \quad (20)$$

Note the arguments of the probability density function above are inconsistent with the original GO-2 form, and provide no consideration of the possibility of up- or down-going intermediate waves. Therefore, this result in (20) is incompatible with the second order geometric optics limit (GO-2) regardless of the kernel used. This result is not surprising when the expansion of the exact spectral Green's function used to derive the original MLA (see [4]) is recalled; in fact the MLA derived result matches GO-2 only when $q_{\xi} = 0$ due to this expansion. This limitation is also apparent due to the fact that the MLA form omits any terms involving q_{ξ} in the phase term of the integrand.

In summary, MLA-based methods can be designed to achieve conformity with the SPM-1, SPM-2, and GO-1 limits, but are inconsistent with the exact GO-2 limit by definition. Because the MLA form is proposed in order to capture non-local effects (as in GO-2) compared to the standard local scattering models, this failure is a cause for concern in applying MLA based methods. Because the MLA is more expensive than standard local scattering models, the gain of using these models is not immediately apparent. Of course, the possibility that equation (20) provides a usable approximation to equation (17) in many cases of practical interest remains. However, use of a method that captures the GO-2 limit by design may offer a higher degree of accuracy in modelling special multiple-scattering effects. One possible solution is to modify the ansatz itself to introduce the vertical component of the scattered ray between two points on the surface ($\pm q_{\xi}$). However in this case the triple integral becomes more coupled and therefore a constant non-local kernel no longer yields a local integral similar to the high-frequency Kirchhoff as in (7). The next section considers a more direct method for achieving agreement in the GO-2 limit.

3. Ray tracing ansatz

As its name indicates, the ray tracing ansatz (RTA) is intuitively based on reflected optical rays at the rough surface. We consider herein only single and double reflection. We assume that for the double reflection, the single reflection model can be convoluted twice. Most models based on iteration of the Kirchhoff approximation can be grouped under this ansatz, see for instance [20], although in the literature many variations are observed involving the use of "shadowing functions". Here we omit any such functions, and further assume that the rough surface is not penetrable or the attenuation in the second medium is important so that no significant number of rays can emerge after penetrating the surface. Evanescent intermediate waves are also not considered in the formulation here.

3.1. Formulation

Begin by writing the scattering amplitude as

$$\mathcal{S}(\mathbf{K}_s, \mathbf{K}_i) = \mathcal{S}_1(\mathbf{K}_s, \mathbf{K}_i) + \mathcal{S}_2(\mathbf{K}_s, \mathbf{K}_i) + \cdots \quad (21)$$

where

$$\mathcal{S}_1(\mathbf{K}_s, \mathbf{K}_i) = \int \phi_1(\mathbf{K}_s, \mathbf{K}_i) \exp[-i(\mathbf{K}_s - \mathbf{K}_i) \cdot \mathbf{X}] d\mathbf{x} \quad (22)$$

and $\mathbf{X} = \mathbf{x} + \eta \hat{z}$. The second iterative term is then expressed explicitly as a product of the first

$$\mathcal{S}_2(\mathbf{K}_s, \mathbf{K}_i) = \int \frac{\mathcal{S}_1(\mathbf{K}_s, \mathbf{K}_\xi) \cdot \mathcal{S}_1(\mathbf{K}_\xi, \mathbf{K}_i) + \mathcal{S}_1(\mathbf{K}_s, \check{\mathbf{K}}_\xi) \cdot \mathcal{S}_1(\check{\mathbf{K}}_\xi, \mathbf{K}_i)}{2q_\xi} d\xi \quad (23)$$

Hence

$$\begin{aligned} \mathcal{S}_2(\mathbf{K}_s, \mathbf{K}_i) &= \iiint \phi_2(\mathbf{K}_s, \mathbf{K}_i; \check{\mathbf{K}}_\xi) \exp[-i(\mathbf{K}_s - \check{\mathbf{K}}_\xi) \cdot \mathbf{X}_1] \exp[-i(\check{\mathbf{K}}_\xi - \mathbf{K}_i) \cdot \mathbf{X}_2] d\xi d\mathbf{x}_1 d\mathbf{x}_2 \\ &+ \iiint \phi_2(\mathbf{K}_s, \mathbf{K}_i; \mathbf{K}_\xi) \exp[-i(\mathbf{K}_s - \mathbf{K}_\xi) \cdot \mathbf{X}_1] \exp[-i(\mathbf{K}_\xi - \mathbf{K}_i) \cdot \mathbf{X}_2] d\xi d\mathbf{x}_1 d\mathbf{x}_2 \end{aligned} \quad (24a)$$

where $\mathbf{K}_\xi = \xi + q_\xi \hat{z}$ and the ‘‘check’’ operator indicates a reversal of the sign of the vertical component of a vector (e.g. $\check{\mathbf{K}}_\xi = \xi - q_\xi \hat{z}$). Using (23), one gets a definition of the second kernel

$$\phi_2(\mathbf{K}_s, \mathbf{K}_i; \mathbf{K}_\xi) = \frac{\phi_1(\mathbf{K}_s, \mathbf{K}_\xi) \cdot \phi_1(\mathbf{K}_\xi, \mathbf{K}_i)}{2|q_\xi|} \quad (25)$$

Note that in the usual Kirchhoff coefficients the incident and the scattered wavenumbers have their vertical components of opposite signs. The two terms in equation (24) account for both down- and up-going intermediate waves, respectively, as is apparent from the arguments in the integrations. It can be shown (see [20]) that the above equations will obtain an ensemble average form identical to the GO-2 ensemble average (equation (17)) when evaluated in the high-frequency limit, due to the explicit inclusion of the q_ξ terms in the intermediate wave phases and the inclusion of both up- and down-going intermediate waves.

If the kernel functions are chosen to satisfy

$$\phi_1(\mathbf{K}_s, \mathbf{K}_i) = \phi_1^T(-\mathbf{K}_i, -\mathbf{K}_s) \quad (26a)$$

$$\phi_2(\mathbf{K}_s, \mathbf{K}_i; \mathbf{K}_\xi) = \phi_2^T(-\mathbf{K}_i, -\mathbf{K}_s; -\mathbf{K}_\xi) \quad (26b)$$

then the RTA ansatz satisfies the principles of reciprocity, vertical and horizontal shift invariance (equation (4)). The unknown kernels in (22) can then be determined from first principles or from matching to fundamental high- and/or low-frequency limits. A first principle approach can be the surface current integral equation or the Stratton-Chu method which may lead to cumbersome kernels [13, 15]. Instead the matching approach is pursued.

3.2. Iterated high-frequency limits

3.2.1. Definitions To produce agreement with the GO-1 and GO-2 kernel functions, the RTA kernel functions are required to be

$$\phi_1(\mathbf{K}_s, \mathbf{K}_i) = \frac{\mathcal{K}(\mathbf{K}_s, \mathbf{K}_i)}{(\mathbf{K}_s - \mathbf{K}_i) \cdot \hat{z}} \quad (27a)$$

$$\phi_2(\mathbf{K}_s, \mathbf{K}_i; \mathbf{K}_\xi) = \frac{1}{2q_\xi} \frac{\mathcal{K}(\mathbf{K}_s, \mathbf{K}_\xi) \cdot \mathcal{K}(\mathbf{K}_\xi, \mathbf{K}_i)}{(\mathbf{K}_s - \mathbf{K}_\xi) \cdot \hat{z} \hat{z} \cdot (\mathbf{K}_\xi - \mathbf{K}_i)} \quad (27b)$$

Note in the above that ϕ_1 is defined with an up-doing first argument and down-going second argument; when evaluated with arbitrary arguments the appropriate substitutions should be made both in the numerator and denominator of the right-hand side of the equation. The sum of S_1 from (22) and S_2 from (24) using the kernels (27) is referred to as the KA-2 model throughout the remainder of this paper.

The tensor multiplication in the second order kernel (for vector scattering problems) translates the physical fact that a reflected ray could take any possible polarization in the transition between the two reflection points while the nominal polarizations of the incident and the scattered waves are imposed by the observer.

Although agreement with GO-1 and GO-2 has been established, the low frequency limit of (22) requires examination.

3.2.2. The “accidental” low-frequency limit In order to verify whether the SPM-1 limit is reached, the following condition must be checked

$$\begin{aligned} \mathcal{B}(\mathbf{K}_s, \mathbf{K}_i) &= \mathcal{K}(\mathbf{K}_s, \mathbf{K}_i) \\ &+ \hat{z} \cdot (\mathbf{K}_s - \mathbf{K}_i) [\phi_2(\mathbf{K}_s, \mathbf{K}_i; \mathbf{K}_i) + \phi_2(\mathbf{K}_s, \mathbf{K}_i; \mathbf{K}_s)] \\ &+ \hat{z} \cdot (\mathbf{K}_s - \check{\mathbf{K}}_i) [\phi_2(\mathbf{K}_s, \mathbf{K}_i; \check{\mathbf{K}}_i) - \phi_2(\mathbf{K}_s, \mathbf{K}_i; \check{\mathbf{K}}_s)] \end{aligned} \quad (28)$$

This condition is obtained by simple linearization of (22) with respect to the surface η . Knowing that

$$\mathcal{K}(\mathbf{K}', \mathbf{K}') = 0 \quad (29)$$

for an arbitrary \mathbf{K}' leads to the following identities

$$\phi_2(\mathbf{K}_s, \mathbf{K}_i; \mathbf{K}_s) = \phi_2(\mathbf{K}_s, \mathbf{K}_i; \mathbf{K}_i) = 0 \quad (30a)$$

$$\phi_2(\mathbf{K}_s, \mathbf{K}_s; \check{\mathbf{K}}_s) = \phi_2(\mathbf{K}_s, \mathbf{K}_s; \mathbf{K}_s) = 0. \quad (30b)$$

for Neumann, Dirichlet, and perfectly conducting surfaces. The last equation ensures that the flat surface response from the local Kirchhoff is not contaminated by the nonlocal part of the ansatz in (22). Using these identities in (28),

$$\mathcal{B}(\mathbf{K}_s, \mathbf{K}_i) = \mathcal{K}(\mathbf{K}_s, \mathbf{K}_i) + (q_k - q_0)\phi_2(\mathbf{K}_s, \mathbf{K}_i; \check{\mathbf{K}}_i) + (q_0 - q_k)\phi_2(\mathbf{K}_s, \mathbf{K}_i; \check{\mathbf{K}}_s) \quad (31)$$

where

$$2(q_k - q_0)\phi_2(\mathbf{K}_s, \mathbf{K}_i; \check{\mathbf{K}}_i) = \mathcal{B}(\mathbf{K}_s, \mathbf{K}_i) - \mathcal{K}(\mathbf{K}_s, \mathbf{K}_i) \quad (32)$$

$$2(q_0 - q_k)\phi_2(\mathbf{K}_s, \mathbf{K}_i; \check{\mathbf{K}}_s) = \mathcal{B}(\mathbf{K}_s, \mathbf{K}_i) - \mathcal{K}(\mathbf{K}_s, \mathbf{K}_i) \quad (33)$$

and therefore the low-frequency limit is formally reached for Dirichlet, Neumann, and perfectly conducting cases. Such a result has been shown in previous works [21, 22]. However, additional expansion of the integrands shows that the SPM-2 limit is not achieved by the model for any of these cases.

It is surprising that the iteration of high-frequency limits used results in convergence toward the SPM-1 limit. A possible explanation could be based on the fact that in the Dirichlet, Neumann, and perfect conductor boundary conditions the high-frequency Kirchhoff (GO-1) coincides with the low-frequency Kirchhoff (tangent plane approximation). However, this coincidence is not observed under general dielectric conditions, so the model developed remains incomplete for the dielectric case. To improve performance for the dielectric case, use of a tangent plane formulation seems attractive in proposing the original kernels of the RTA. However, there are several deficits in the tangent plane approximation with regard to reciprocity and time reversal properties. Although some manifestly reciprocal formulations of the tangent plane approximation have been proposed (see for instance equation 4.12 in [23]), the resulting expressions are cumbersome and complicated. An alternative solution that avoids these difficulties is proposed in the next section.

4. The nonlocal weighted curvature approximation

An interesting alternative to a reciprocal tangent plane approximation is the Weighted Curvature Approximation (WCA) (see equation 24 in [6]). The local WCA yields the proper low and high frequency limits while remaining reciprocal and compact. Under the 3D notation introduced in the previous sections, the local WCA (WCA-1) can be recast as

$$\mathcal{S}(\mathbf{K}_s, \mathbf{K}_i) = \frac{1}{(\mathbf{K}_s - \mathbf{K}_i) \cdot \hat{\mathbf{z}}} \int \mathcal{G}(\mathbf{K}_s, \mathbf{K}_i; \nabla\eta) \exp[-i(\mathbf{K}_s - \mathbf{K}_i) \cdot \mathbf{X}] d\mathbf{x} \quad (34)$$

where

$$\mathcal{G}(\mathbf{K}_s, \mathbf{K}_i; \nabla\eta) = \mathcal{B}(\mathbf{K}_s, \mathbf{K}_i) - \mathcal{T}(\mathbf{K}_s, \mathbf{K}_i; -Q_z \nabla\eta) \quad (35)$$

$$\mathcal{T}(\mathbf{K}_s, \mathbf{K}_i; -Q_z \nabla\eta) = \mathcal{B}(\widetilde{\mathbf{K}}_s, \widetilde{\mathbf{K}}_i) - \mathcal{K}(\widetilde{\mathbf{K}}_s, \widetilde{\mathbf{K}}_i) \quad (36)$$

The local WCA is derived as a simplification of the local-curvature approximation (LCA), which has a more complex form similar to the SSA-2 theory [3]; see [6] for the complete LCA expressions.

A nonlocal model based on an iterated WCA has the form defined in (21) with first and second order kernels

$$\phi_1(\mathbf{K}_s, \mathbf{K}_i) = \frac{\mathcal{G}(\mathbf{K}_s, \mathbf{K}_i; \nabla\eta)}{(\mathbf{K}_s - \mathbf{K}_i) \cdot \hat{\mathbf{z}}} \quad (37a)$$

$$\phi_2(\mathbf{K}_s, \mathbf{K}_i; \mathbf{K}_\xi) = \frac{1}{2q_\xi} \frac{\mathcal{G}(\mathbf{K}_s, \mathbf{K}_\xi; \nabla\eta_1) \cdot \mathcal{G}(\mathbf{K}_\xi, \mathbf{K}_i; \nabla\eta_2)}{(\mathbf{K}_s - \mathbf{K}_\xi) \cdot \hat{\mathbf{z}} \hat{\mathbf{z}} \cdot (\mathbf{K}_\xi - \mathbf{K}_i)} \quad (37b)$$

Due to the RTA basis of this method, predicted ensemble average cross sections remain consistent with the GO-2 basic form. In addition, the nonlocal WCA (WCA-1+NLWCA-2) should introduce better treatment of low-frequency limits under general dielectric conditions. Due to the quadratic nature of the curvature kernel itself (35) [6], it can be shown that the SPM-1 limit achieved by WCA-1 is not contaminated by the

nonlocal contribution. Thus both GO-1 and SPM-1 limits are now achieved from local considerations alone, while nonlocal effects contribute toward the GO-2 and perhaps the SPM-2 limit. This model is called the iterated or nonlocal weighted curvature approximation.

5. The SPM-2 limit

It is important to check the second-order low frequency limit or SPM-2 of this iterated model. For the NLWCA-2 term, the phases in the second-order WCA will not contribute since the kernels themselves have at lowest order a quadratic dependence on the surface. Hence, by expanding (37) we get,

$$\phi_2(\mathbf{K}_s, \mathbf{K}_i; \mathbf{K}_\xi) \approx \frac{1}{2q_\xi} \frac{[\nabla\eta_1 \cdot \nabla\nabla\mathcal{G}(\mathbf{K}_s, \mathbf{K}_\xi; \mathbf{0}) \cdot \nabla\eta_1] \cdot \mathcal{G}(\mathbf{K}_\xi, \mathbf{K}_i; \mathbf{0})}{(\mathbf{K}_s - \mathbf{K}_\xi) \cdot \hat{z}\hat{z} \cdot (\mathbf{K}_\xi - \mathbf{K}_i)} \quad (38a)$$

$$\phi_2(\mathbf{K}_s, \mathbf{K}_i; \check{\mathbf{K}}_\xi) \approx \frac{1}{2q_\xi} \frac{\mathcal{G}(\mathbf{K}_s, \check{\mathbf{K}}_\xi; \mathbf{0}) \cdot [\nabla\eta_2 \cdot \nabla\nabla\mathcal{G}(\check{\mathbf{K}}_\xi, \mathbf{K}_i; \mathbf{0}) \cdot \nabla\eta_2]}{(\mathbf{K}_s - \check{\mathbf{K}}_\xi) \cdot \hat{z}\hat{z} \cdot (\check{\mathbf{K}}_\xi - \mathbf{K}_i)} \quad (38b)$$

When integrating over \mathbf{x}_1 , \mathbf{x}_2 , and ξ the previous kernels will vanish one by one. This leaves the SPM-2 contribution only coming from WCA-1. However it has been shown that the WCA-1 fails to reproduce SPM-2 [6]. Although perhaps a third iteration of the RTA could improve this limitation, such a model would be too costly and is not recommended. Therefore one must live with the fact that the double scattering WCA does not reproduce the formal SPM-2 limit.

6. Tilt invariance

Because the WCA-1 has been shown to be tilt invariant [6, 19, 24], it is relevant to check that the nonlocal kernel in (37) of NLWCA-2 does not contaminate the local response under scattering from a slightly tilted, slightly-rough surface. In other words, it is desired to show that the NLWCA-2 term does not contribute in the SPM-1 limit even for a tilted slightly rough surface.

Let us study the behavior of the nonlocal kernel (37) under a slight tilt so the following substitution is operated

$$\eta(\mathbf{x}) \Rightarrow \eta(\mathbf{x}) + \vec{a} \cdot \mathbf{x} \quad (39)$$

and hence

$$\phi_2(\mathbf{K}_s, \mathbf{K}_i; \mathbf{K}_\xi) = \frac{1}{2q_\xi} \frac{\mathcal{G}(\mathbf{K}_s, \mathbf{K}_\xi; \nabla\eta_1 + \vec{a}) \cdot \mathcal{G}(\mathbf{K}_\xi, \mathbf{K}_i; \nabla\eta_2 + \vec{a})}{(\mathbf{K}_s - \mathbf{K}_\xi) \cdot \hat{z}\hat{z} \cdot (\mathbf{K}_\xi - \mathbf{K}_i)} \quad (40a)$$

$$\phi_2(\mathbf{K}_s, \mathbf{K}_i; \check{\mathbf{K}}_\xi) = \frac{1}{2q_\xi} \frac{\mathcal{G}(\mathbf{K}_s, \check{\mathbf{K}}_\xi; \nabla\eta_1 + \vec{a}) \cdot \mathcal{G}(\check{\mathbf{K}}_\xi, \mathbf{K}_i; \nabla\eta_2 + \vec{a})}{(\mathbf{K}_s - \check{\mathbf{K}}_\xi) \cdot \hat{z}\hat{z} \cdot (\check{\mathbf{K}}_\xi - \mathbf{K}_i)} \quad (40b)$$

and the linearization in η and in \vec{a} yield

$$\phi_2(\mathbf{K}_s, \mathbf{K}_i; \mathbf{K}_\xi) \approx \frac{1}{2q_\xi} \frac{[\nabla\mathcal{G}(\mathbf{K}_s, \mathbf{K}_\xi; \vec{a}) \cdot \nabla\eta_1] \cdot \mathcal{G}(\mathbf{K}_\xi, \mathbf{K}_i; \mathbf{0})}{(\mathbf{K}_s - \mathbf{K}_\xi) \cdot \hat{z}\hat{z} \cdot (\mathbf{K}_\xi - \mathbf{K}_i)} \quad (41a)$$

$$\phi_2(\mathbf{K}_s, \mathbf{K}_i; \check{\mathbf{K}}_\xi) \approx \frac{1}{2q_\xi} \frac{\mathcal{G}(\mathbf{K}_s, \check{\mathbf{K}}_\xi; \mathbf{0}) \cdot [\nabla \mathcal{G}(\check{\mathbf{K}}_\xi, \mathbf{K}_i; \vec{a}) \cdot \nabla \eta_2]}{(\mathbf{K}_s - \check{\mathbf{K}}_\xi) \cdot \hat{z} \hat{z} \cdot (\check{\mathbf{K}}_\xi - \mathbf{K}_i)} \quad (41b)$$

These two kernels will cancel each other when inserted into the nonlocal contribution in (22). It is therefore demonstrated that WCA-1+NLWCA-2 is tilt invariant up to the first order in the tiling vector. To our knowledge, the only multiple scattering models in the literature that ensure tilt invariance are the NLCA in [24], NLSSA with the new kernel in (16) and the iterated or nonlocal WCA (WCA-1+NLWCA-2) developed in this paper (37).

7. Numerical examples

To examine the performance of the models considered in this paper, along with standard local scattering models, a study was performed of scattering from a one-dimensional sinusoidal grating under Dirichlet boundary conditions. Results are presented in terms of bistatically scattered Floquet mode amplitudes in the plane of the grating; these Floquet modes satisfy the grating relation

$$k = k_0 + \frac{2\pi n}{P} \quad (42)$$

where n is the mode number. Mode amplitudes (labelled as $|E|$ in the Figures) are normalized such that the sum of the amplitude squared of all mode amplitudes is unity. Both “single” and “double” gratings are considered, where the surface profile $z(x)$ of a “single” grating is defined as

$$z(x) = A \sin\left(\frac{2\pi x}{P}\right) \quad (43)$$

where $z(x)$ is the surface profile, A is the sine wave amplitude, and P its period. For a “double” grating

$$z(x) = A \sin\left(\frac{2\pi x}{P}\right) + A_2 \sin\left(\frac{2\pi x}{P_2} - \Phi\right) \quad (44)$$

In all the results illustrated, the incident wave approaches at an angle of 0.5 radians with respect to the x axis.

A numerical “method of moments” algorithm was used to provide exact results for comparison; the algorithm was based on the procedure described in [25], and showed good convergence at a sample rate of approximately 10 points per wavelength for surface fields.

Figures 1 and 2 plot the results for the case $A = 0.5\lambda$, $P = 5\lambda$. This case was previously considered in [4], although information was provided in this reference only in terms of the level of power conservation observed. Information on power conservation is provided for each method here in the legends of the figures. Figure 1 includes the local models KA (or GO-1), SSA-1, SSA-2 [3], LCA [6], and WCA, while Figure 2 plots the results for the MLA using the kernels (6) (NLSSA), (13) (MLM), and (16) (modified NLSSA or MNLSSA). Results from the RTA are also plotted including the KA-2 (27)

and WCA-1+NLWCA-2. This case is approaching a KA type surface, although the surface amplitude and period remain moderate on a wavelength scale. Results show the local models to perform very well, with the exception of the -1 mode where some higher-order scattering effects potentially influence the results. For this mode the SSA-2, LCA, and WCA-1 show improved performance compared to KA, but complete agreement is still not achieved by these models. SSA-1 performance is found inadequate at almost all angles, due to the failure of SSA-1 to reproduce KA. The LCA also shows poor performance for mode 0, although the reason for this failure is not immediately clear.

Figure 2 shows the non-local models also to perform well, and to achieve an improved prediction of the -1 mode in most cases. NLSSA and MNLSSA show very similar performance, while the MLM is less accurate in general. The NLWCA performs well also, although in some cases the NLWCA-2 correction moves the original WCA-1 away from the correct result. KA-2 is shown to produce little change from the original KA-2 predictions, except an increased error is observed for mode -1 . These results indicate that the -1 mode likely has contributions beyond those of a simple ray-tracing algorithm, so that improved spectral accuracy (such as the SPM-2 limit of NLSSA and MNLSSA) is advantageous in this case.

Figures 3 and 4 show similar results for the case $A = \lambda$, $P = 20\lambda$. In this larger period case, the RTA models may be expected to show improved performance. Although scattering exists at from modes -37 to 2 in this case, only modes -20 to 2 are plotted due to the extremely small fields at larger angles. Again the local models are seen to perform very well, although here mode -4 presents some difficulties and is not well predicted by KA. Figure 4 shows that most of the non-local models also fail to capture this mode, although KA-2 shows a correction in the right direction. In general, conclusions for this case are similar to those of Figures 1 and 2.

Finally, Figures 5 and 6 consider a double grating, with $A = \lambda$, $P = 20\lambda$, $A_2 = 0.03\lambda$, $P_2 = \lambda$, and $\Phi = \pi/3$. This case contains both large and small scale surfaces, so that some approximate multi-scale scattering effects can be observed. In particular, the SPM-1 theory for this surface would indicate a contribution around mode -20 due to the small scale surface. Results in Figure 5 indeed show an increased scattering level around mode -20 , and a complex scattering pattern in general. Again the local models all yield a reasonable performance, although the KA-1 model shows increased error in the vicinity of mode -20 . All models have difficulty predicting the results for modes more negative than -30 . The non-local models in Figure 4 show somewhat improved performance in matching this region, particularly the KA-2 method. This is in agreement with the expectation that KA-2 captures the SPM-1 limit for the Dirichlet case.

8. Conclusion

We have analyzed two families of nonlocal scattering models. The first is based on the Meecham-Lysanov ansatz (MLA). The second family is inspired by iteration of the

geometric optics (GO) and is called the ray tracing ansatz (RTA). For the MLA, the first deficiency we identified is that the first order geometric optics limit (GO-1) is not attained by NLSSA contrary to the statement in [4]. As an alternative, we proposed two kernels. The first ensures both the small perturbation method (SPM-1) and GO-1 limits but with no constraint to the SPM-2. This new kernel is in (13) which is a generalization and a simplification of the first-order operator expansion method (OEM-1) in [5, 18] and the Meecham-Lysanov model itself [3]. It is also possible to derive a more complete kernel as in (16) which for Dirichlet, Neumann, and perfectly conducting boundaries ensures both the GO-1 and SPM-1 limits as well as SPM-2 and tilt invariance. It is however interesting to notice that even with this new kernel in (16) the GO-2 limit will never be reached due to a deficiency in the MLA or NLSSA ansatz itself.

For this reason we moved to the second family of nonlocal models. We showed that iteration of the high-frequency Kirchhoff can provide not only GO-1 and GO-2 but also SPM-1 by accident from the nonlocal contribution in the Dirichlet, Neumann, and perfectly conducting cases. However under general dielectric conditions the SPM-1 limit is not achieved. We examined the weighted curvature approximation WCA [6] as an alternative to a general low-frequency Kirchhoff approximation. A non-local WCA (WCA-1+NLWCA-2) (37) was developed along the lines of the ray tracing ansatz, and is very powerful since it retains most limits such as GO-1, GO-2, and SPM-1 as well as staying tilt invariant, reciprocal and compact. NLWCA also solves an inconsistency in previous models as to the need for the nonlocal correction to retrieve the local SPM-1 limit. The SPM-2 limit is not formally reached by WCA-1+NLWCA-2 while the GO-2 limit is not reached by the NLSSA even with the kernel in (16). A study of scattering from sinusoidal gratings provided some indication that the relative importance of matching the GO-2 or SPM-2 limits can depend on the scattering problem considered.

Acknowledgments

We would like to express our gratitude to our colleagues Charles-Antoines Gu erin and Mark Saillard for helpful comments and suggestions.

9. Appendix: Kirchhoff and SPM kernel definitions and identities

For the Neumann-Dirichlet cases, the \mathcal{K} and \mathcal{B} functions are

$$\mathcal{K}(\mathbf{k}, \mathbf{k}_0) = \left([K^2 - \mathbf{k} \cdot \mathbf{k}_0 + q_k q_0], \quad -[K^2 - \mathbf{k} \cdot \mathbf{k}_0 + q_k q_0] \right) \quad (45a)$$

$$\mathcal{B}(\mathbf{k}, \mathbf{k}_0) = \left(2[K^2 - \mathbf{k} \cdot \mathbf{k}_0], \quad -2q_k q_0 \right) \quad (45b)$$

For the perfect conductor case, we have

$$\mathcal{K}(\mathbf{k}; \mathbf{k}_0) = \begin{pmatrix} [(K^2 + q_k q_0)\hat{\mathbf{k}} \cdot \hat{\mathbf{k}}_0 - k k_0] & K(q_k + q_0)(\hat{\mathbf{k}} \times \hat{\mathbf{k}}_0) \cdot \hat{\mathbf{z}} \\ K(q_k + q_0)(\hat{\mathbf{k}}_0 \times \hat{\mathbf{k}}) \cdot \hat{\mathbf{z}} & -[(K^2 + q_k q_0)\hat{\mathbf{k}} \cdot \hat{\mathbf{k}}_0 - k k_0] \end{pmatrix} \quad (46)$$

$$\mathcal{B}(\mathbf{k}; \mathbf{k}_0) = 2 \begin{pmatrix} K^2 \hat{\mathbf{k}} \cdot \hat{\mathbf{k}}_0 - k k_0 & K q_0 (\hat{\mathbf{k}} \times \hat{\mathbf{k}}_0) \cdot \hat{\mathbf{z}} \\ K q_k (\hat{\mathbf{k}}_0 \times \hat{\mathbf{k}}) \cdot \hat{\mathbf{z}} & -q_k q_0 \hat{\mathbf{k}} \cdot \hat{\mathbf{k}}_0 \end{pmatrix} \quad (47)$$

The SPM-2 kernel for both cases can be defined as

$$\mathcal{B}_2(\mathbf{k}, \mathbf{k}_0; \boldsymbol{\xi}) = \frac{\mathcal{B}(\mathbf{k}, \boldsymbol{\xi}) \mathcal{B}(\boldsymbol{\xi}, \boldsymbol{\xi}) \mathcal{B}(\boldsymbol{\xi}, \mathbf{k}_0)}{4 Q_z q_\xi^2} \quad (48)$$

See [6] for definitions of the polarization vectors in the perfectly conducting case. Note there is a difference in the normalization between our notation and that of Voronovich [3] that is essentially a factor of $2q_k q_0$ for the SPM-1 and Kirchhoff coefficients and a factor of $-q_k q_0 / Q_z$ for the SPM-2 coefficient.

The following identities are useful in finding the limits discussed in the paper:

$$\mathcal{B}_2(\mathbf{k}, \mathbf{k}_0; \mathbf{k}) + \mathcal{B}_2(\mathbf{k}, \mathbf{k}_0; \mathbf{k}_0) = \mathcal{B}(\mathbf{k}, \mathbf{k}_0) \quad (49a)$$

$$q_k \mathcal{B}_2(\mathbf{k}, \mathbf{k}_0; \mathbf{k}) + q_0 \mathcal{B}_2(\mathbf{k}, \mathbf{k}_0; \mathbf{k}_0) = \frac{q_k^2 + q_0^2}{q_k + q_0} \mathcal{B}(\mathbf{k}, \mathbf{k}_0) \quad (49b)$$

$$q_0 \mathcal{B}_2(\mathbf{k}, \mathbf{k}_0; \mathbf{k}) + q_k \mathcal{B}_2(\mathbf{k}, \mathbf{k}_0; \mathbf{k}_0) = \frac{2q_k q_0}{q_k + q_0} \mathcal{B}(\mathbf{k}, \mathbf{k}_0) \quad (49c)$$

$$\frac{1}{2} [\nabla \mathcal{B}_2(\mathbf{k}, \mathbf{k}_0; \mathbf{k}) + \nabla \mathcal{B}_2(\mathbf{k}, \mathbf{k}_0; \mathbf{k}_0)] \cdot \mathbf{Q}_H = \frac{q_k - q_0}{q_k + q_0} \mathcal{K}(\mathbf{k}, \mathbf{k}_0) \quad (49d)$$

$$\frac{1}{2} [\nabla \mathcal{B}_2(\mathbf{k}, \mathbf{k}_0; \mathbf{k}) - \nabla \mathcal{B}_2(\mathbf{k}, \mathbf{k}_0; \mathbf{k}_0)] \cdot \mathbf{Q}_H = \mathcal{B}(\mathbf{k}, \mathbf{k}_0) - \mathcal{K}(\mathbf{k}, \mathbf{k}_0) \quad (49e)$$

$$[q_k \nabla \mathcal{B}_2(\mathbf{k}, \mathbf{k}_0; \mathbf{k}) - q_0 \nabla \mathcal{B}_2(\mathbf{k}, \mathbf{k}_0; \mathbf{k}_0)] \cdot \frac{\mathbf{Q}_H}{Q_z} = \mathcal{B}(\mathbf{k}, \mathbf{k}_0) - \frac{4q_k q_0}{(q_k + q_0)^2} \mathcal{K}(\mathbf{k}, \mathbf{k}_0) \quad (49f)$$

$$[q_0 \nabla \mathcal{B}_2(\mathbf{k}, \mathbf{k}_0; \mathbf{k}) - q_k \nabla \mathcal{B}_2(\mathbf{k}, \mathbf{k}_0; \mathbf{k}_0)] \cdot \frac{\mathbf{Q}_H}{Q_z} = \mathcal{B}(\mathbf{k}, \mathbf{k}_0) - \frac{2(q_k^2 + q_0^2)}{(q_k + q_0)^2} \mathcal{K}(\mathbf{k}, \mathbf{k}_0) \quad (49g)$$

$$\frac{1}{2} \mathbf{Q}_H \cdot [\nabla \nabla \mathcal{B}_2(\mathbf{k}, \mathbf{k}_0; \mathbf{k}) + \nabla \nabla \mathcal{B}_2(\mathbf{k}, \mathbf{k}_0; \mathbf{k}_0)] \cdot \mathbf{Q}_H = 2(\mathcal{B}(\mathbf{k}, \mathbf{k}_0) - \mathcal{K}(\mathbf{k}, \mathbf{k}_0)) \quad (49h)$$

$$\frac{1}{2} \mathbf{Q}_H \cdot [q_k^2 \nabla \nabla \mathcal{B}_2(\mathbf{k}, \mathbf{k}_0; \mathbf{k}) + q_0^2 \nabla \nabla \mathcal{B}_2(\mathbf{k}, \mathbf{k}_0; \mathbf{k}_0)] \cdot \mathbf{Q}_H = (q_k^2 + q_0^2) (\mathcal{B}(\mathbf{k}, \mathbf{k}_0) - \mathcal{K}(\mathbf{k}, \mathbf{k}_0)) \quad (49i)$$

The first equation in (49) is a well known property formally obtainable from the shift invariance to first order of the SPM-2 itself, see equation 3.16 [4]. The remaining equations in (49) are rather very complicated to demonstrate in general. With the exception of the final two equations, we have verified them for Neumann, Dirichlet, and perfect conductor cases. In the general dielectric case, these equations may not hold formally but they could be used approximately to within the quadratic order in ($\mathbf{Q}_H = \mathbf{k} - \mathbf{k}_0$). This order of approximation is often sufficient since the difference between the low and high limits is at least quadratic in \mathbf{Q}_H , see [6]. The final two equations are valid only up to the quadratic order in \mathbf{Q}_H even for the Neumann, Dirichlet, and perfect conductor cases.

References

- [1] W. C. Meecham, “Fourier transform method for the treatment of the problem of the reflection of radiation from irregular surfaces,” *J. Acoust. Soc. America*, vol. 28, pp. 370–377, 1956.
- [2] Y. P. Lysanov, “About one approximate solution of the problem of acoustic wave scattering by a rough interface,” *Sov. Phys. Acoust.*, vol. 2, pp. 190–198, 1956, Engl. Transl.
- [3] A. G. Voronovich, *Wave scattering from rough surfaces*, second updated ed. Tiergartenstrasse 17, D-69121 Heidelberg, Germany: Springer-Verlag, 1994, 236 pages.
- [4] —, “Non-local small-slope approximation for wave scattering from rough surfaces,” *Waves in Random Media*, vol. 6, pp. 151–167, 1996.
- [5] D. M. Milder, “An improved formalism for wave scattering from rough surface,” *J. Acoust. Soc. America*, vol. 89, no. 2, pp. 529–541, 1991.
- [6] T. Elfouhaily, S. Guignard, R. Awadallah, and D. R. Thompson, “Local and non-local curvature approximation: a new asymptotic theory for wave scattering,” *Waves in Random Media*, vol. 13, no. 4, pp. 321–337, 2003.
- [7] V. I. Tatarskii, “Phase factors representation for electromagnetic scattering from a rough-surface perfect conductor,” *Waves in Random Media*, vol. 10, pp. 339–358, 2000.
- [8] N. Garcia, V. Celli, and M. Nieto-Vesperinas, “Exact multiple scattering of waves from random rough surfaces,” *Opt. Comm.*, vol. 30, pp. 279–281, 1979.
- [9] Y.-Q. Jin and M. Lax, “Backscattering enhancement from a randomly rough surface,” *Phys. Rev. B*, vol. 42, no. 16, pp. 9819–9829, 1990.
- [10] C. Macaskill, “Geometric optics and enhanced backscatter from very rough surfaces,” *J. Opt. Soc. America*, vol. 8, pp. 88–96, 1991.
- [11] A. Ishimaru and J. S. Chen, “Scattering from very rough metallic and dielectric surfaces: a theory based on the modified kirchhoff approximation,” *Waves in Random Media*, vol. 1, pp. 21–34, 1991.
- [12] A. K. Fung, *Microwave scattering and emission model and their applications*. Artech House, 685 Canton Street, Norwood, MA, 1994, 573 pages.
- [13] J. L. Álvarez-Pérez, “An extension of the IEM/IEEM surface scattering model,” *Waves in Random Media*, vol. 11, pp. 307–329, 2001.
- [14] T. Elfouhaily, D. R. Thompson, D. E. Freund, D. Vandemark, and B. Chapron, “A new bistatic model for electromagnetic scattering from perfectly conducting random surfaces: numerical evaluation and comparison with SPM,” *Waves in Random Media*, vol. 11, pp. 33–43, 2001.
- [15] K. S. Chen, T. D. Wu, L. Tsang, J. C. Shi, and A. K. Fung, “Emission of rough surfaces calculated by the integral equation method with comparison to three-dimensional moment method simulations,” *IEEE Trans. Geosci. and Remote Sens.*, vol. 41, no. 1, pp. 90–101, 2003.
- [16] D. M. Milder, “Role of the admittance operator in rough-surface scattering,” *J. Acoust. Soc. America*, vol. 100, no. 2, pp. 759–768, 1996.
- [17] A. G. Voronovich, “Small-slope approximation for electromagnetic wave scattering at a rough interface of two dielectric half-spaces,” *Waves in Random Media*, vol. 4, pp. 337–367, 1994.
- [18] D. M. Milder, “An improved formalism for electromagnetic scattering from a perfectly conducting rough surface,” *Radio Sci.*, vol. 31, no. 6, pp. 1369–1376, 1996.
- [19] T. Elfouhaily, S. Guignard, and D. R. Thompson, “Formal tilt invariance of the local curvature approximation,” *Waves in Random Media*, vol. 13, pp. L7–L11, 2003.
- [20] C. Bourlier and G. Berginc, “Multiple scattering in the high-frequency limit with second-order shadowing function from 2-d anisotropic rough dielectric surfaces. part i. theoretical study,” *Waves in Random Media*, 2004, in press.
- [21] D. Holliday, “Resolution of a controversy surrounding the Kirchhoff approach and the small perturbation method in rough surface scattering theory,” *IEEE Trans. Antennas Propag.*, vol. AP-35, no. 1, pp. 120–122, Jan. 1987.
- [22] T. Elfouhaily, D. R. Thompson, B. Chapron, and D. Vandemark, “A new bistatic model for

- electromagnetic scattering from perfect conducting random surfaces,” *Waves in Random Media*, vol. 9, pp. 281–294, 1999.
- [23] R. Dashen and D. Wurmser, “A new theory for scattering from a surface,” *J. Math. Phys.*, vol. 32, no. 4, pp. 971–985, 1991.
- [24] T. Elfouhaily, S. Guignard, and D. R. Thompson, “Formal tilt invariance of the non-local curvature approximation and its connection to the integral equation method,” *IEEE TGARS Letters*, 2004, in press.
- [25] M. E. Veysoglu, H. A. Yueh, R. T. Shin, and J. A. Kong, “Polarimetric passive remote sensing of periodic surfaces,” *J. Electromagn. Waves and Appl.*, vol. 5, pp. 267–280, 1991.

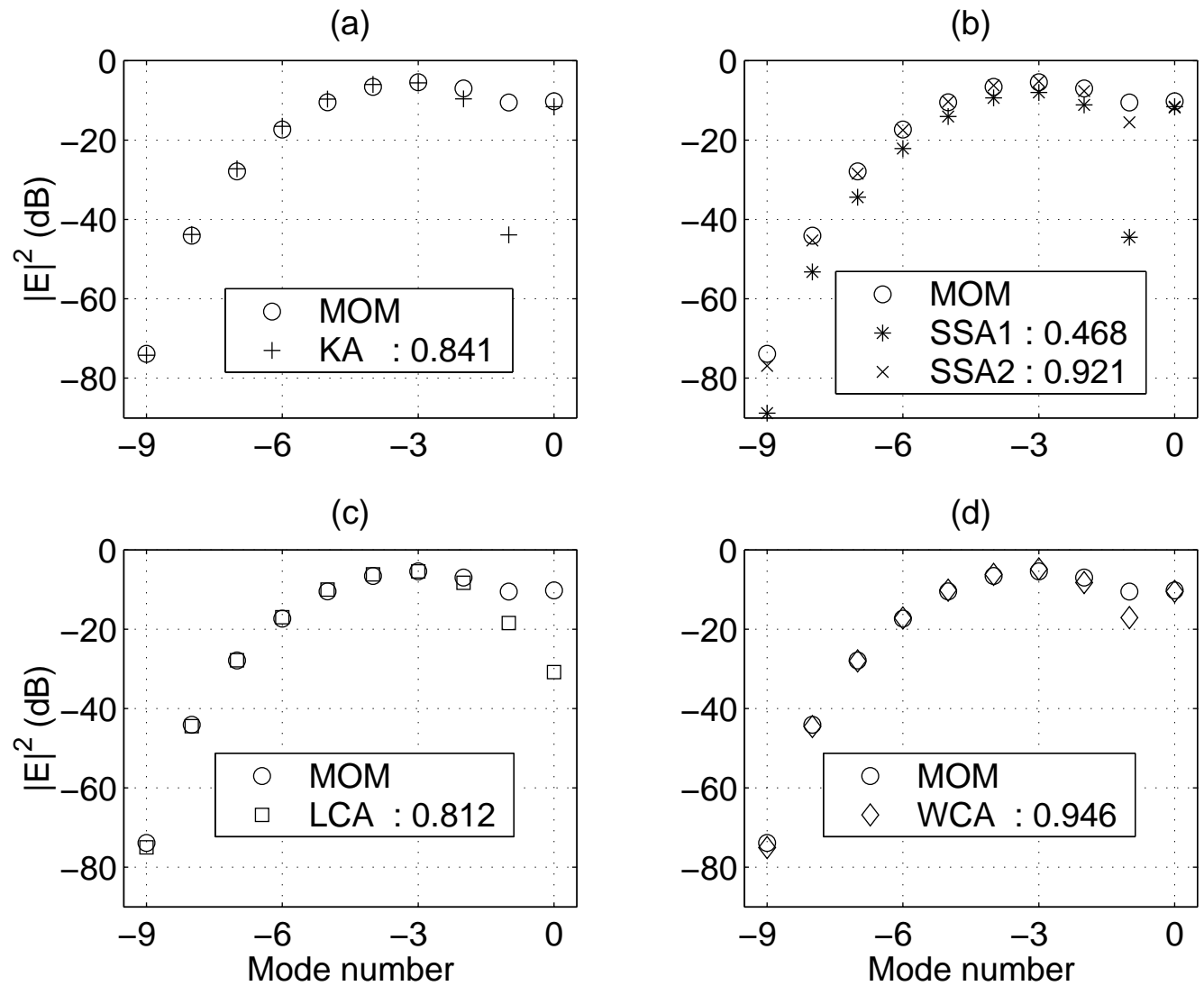


Figure 1. Comparison between rigorous and local approximate models for $A = 0.5\lambda$, $P = 5\lambda$ (a) MoM and Kirchhoff (b) MOM, SSA1, and SSA2 (c) MOM and LCA (d) MOM and WCA-1

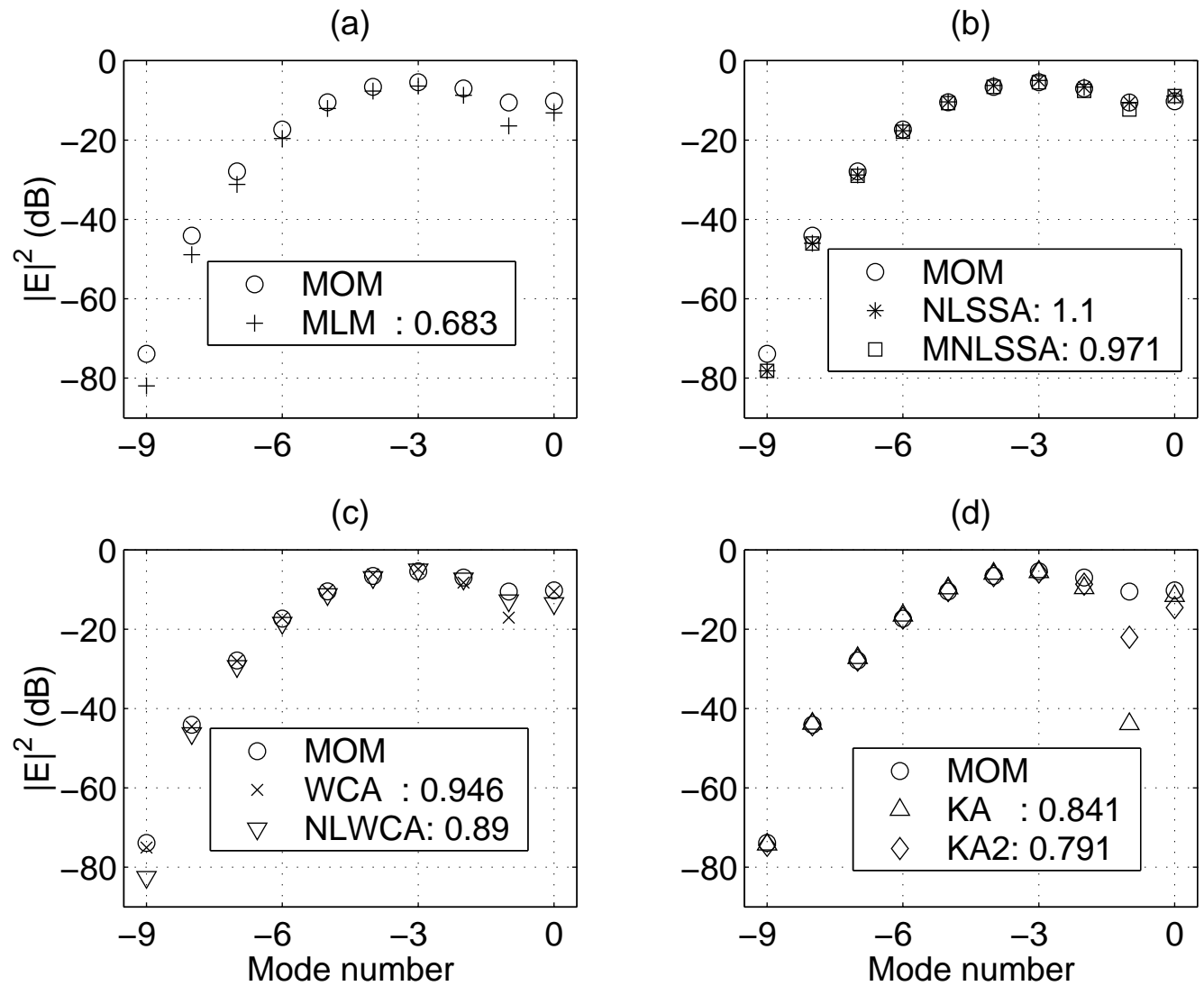


Figure 2. Comparison between rigorous and non-local approximate models for $A = 0.5\lambda$, $P = 5\lambda$ (a) MoM and MLM (b) MOM, NLSSA, and MNLSSA (c) MOM, WCA-1, and WCA-1+NLWCA-2 (d) MOM, KA, and KA-2

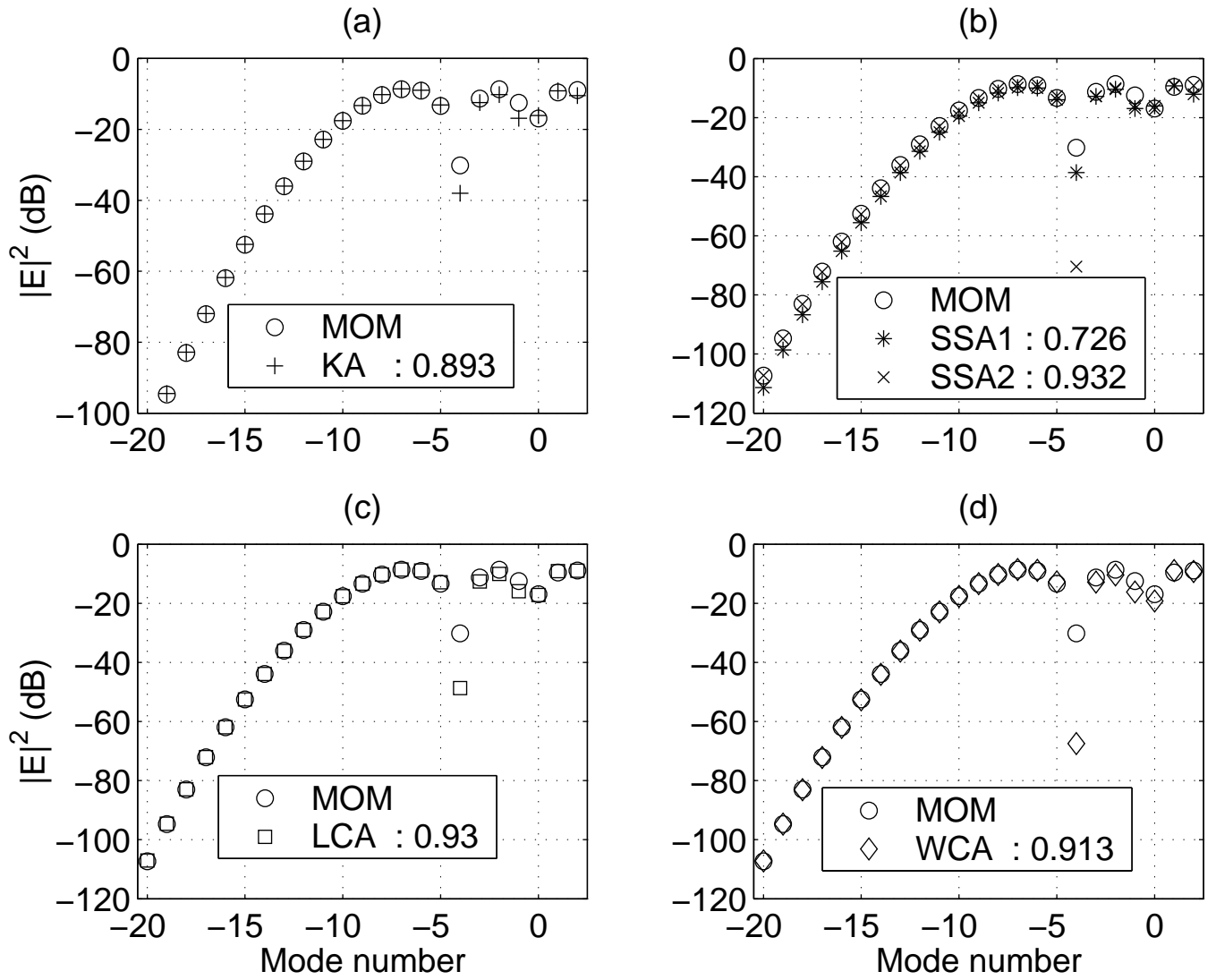


Figure 3. Comparison between rigorous and local approximate models for $A = \lambda$, $P = 20\lambda$ (a) MoM and Kirchhoff (b) MOM, SSA1, and SSA2 (c) MOM and LCA (d) MOM and WCA-1

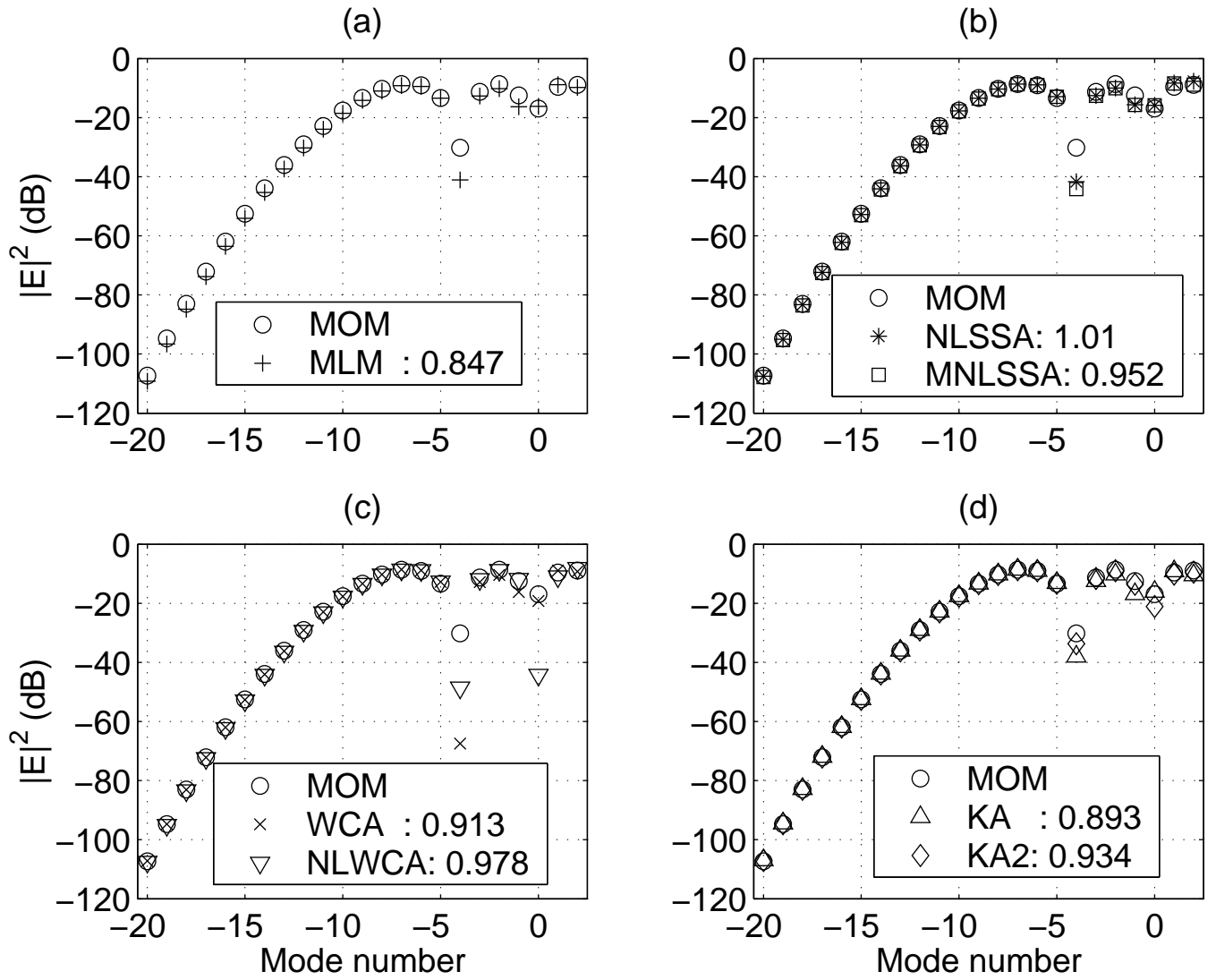


Figure 4. Comparison between rigorous and nonlocal approximate models for $A = \lambda$, $P = 20\lambda$ (a) MoM and MLM (b) MOM, NLSSA, and MNLSSA (c) MOM, WCA-1, and WCA-1+NLWCA-2 (d) MOM, KA, and KA-2

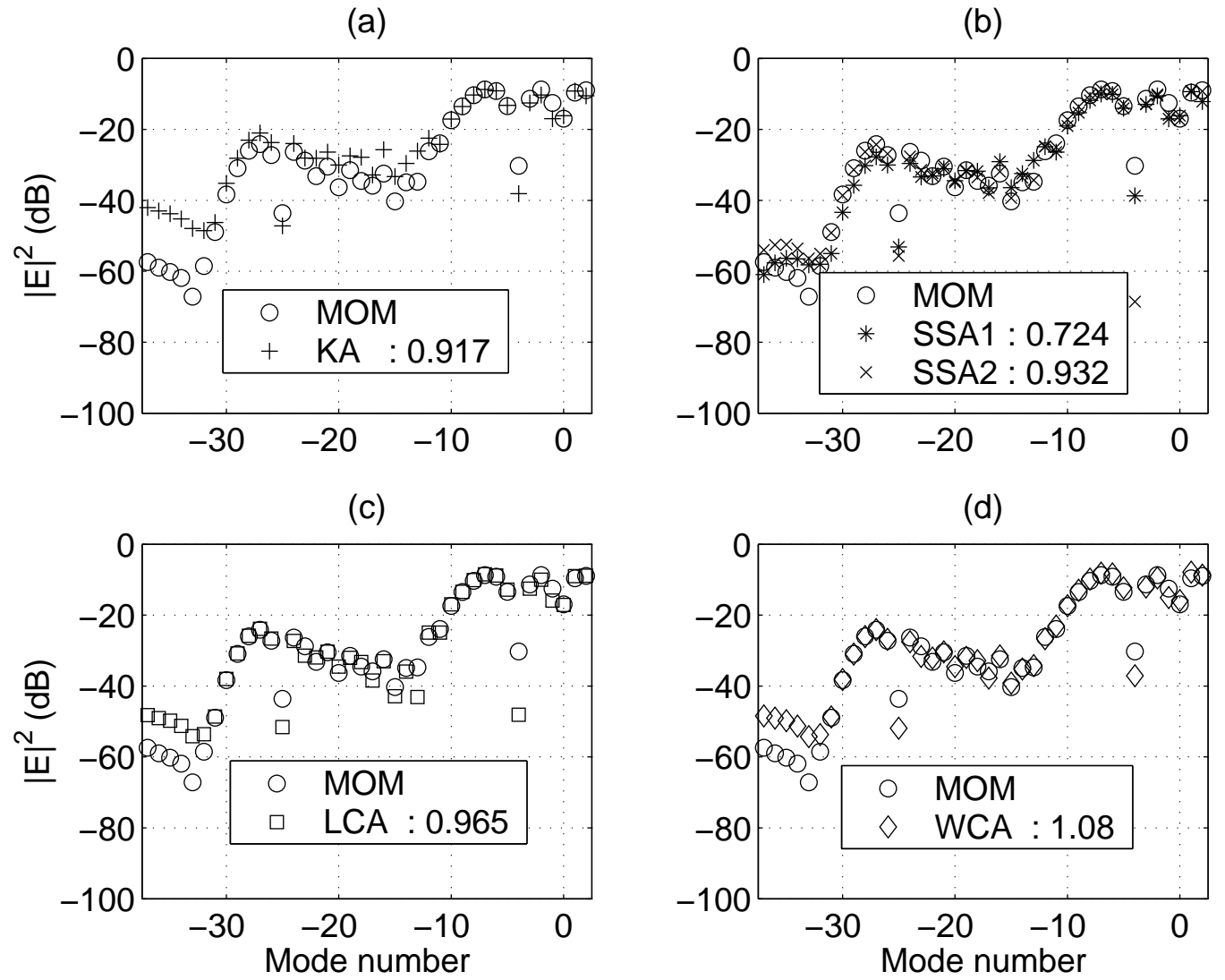


Figure 5. Comparison between rigorous and local approximate models for $A = \lambda$, $P = 20\lambda$, $A_2 = 0.03\lambda$, $P_2 = \lambda$, $\Phi = \pi/3$ (a) MoM and Kirchhoff (b) MOM, SSA1, and SSA2 (c) MOM and LCA (d) MOM and WCA-1

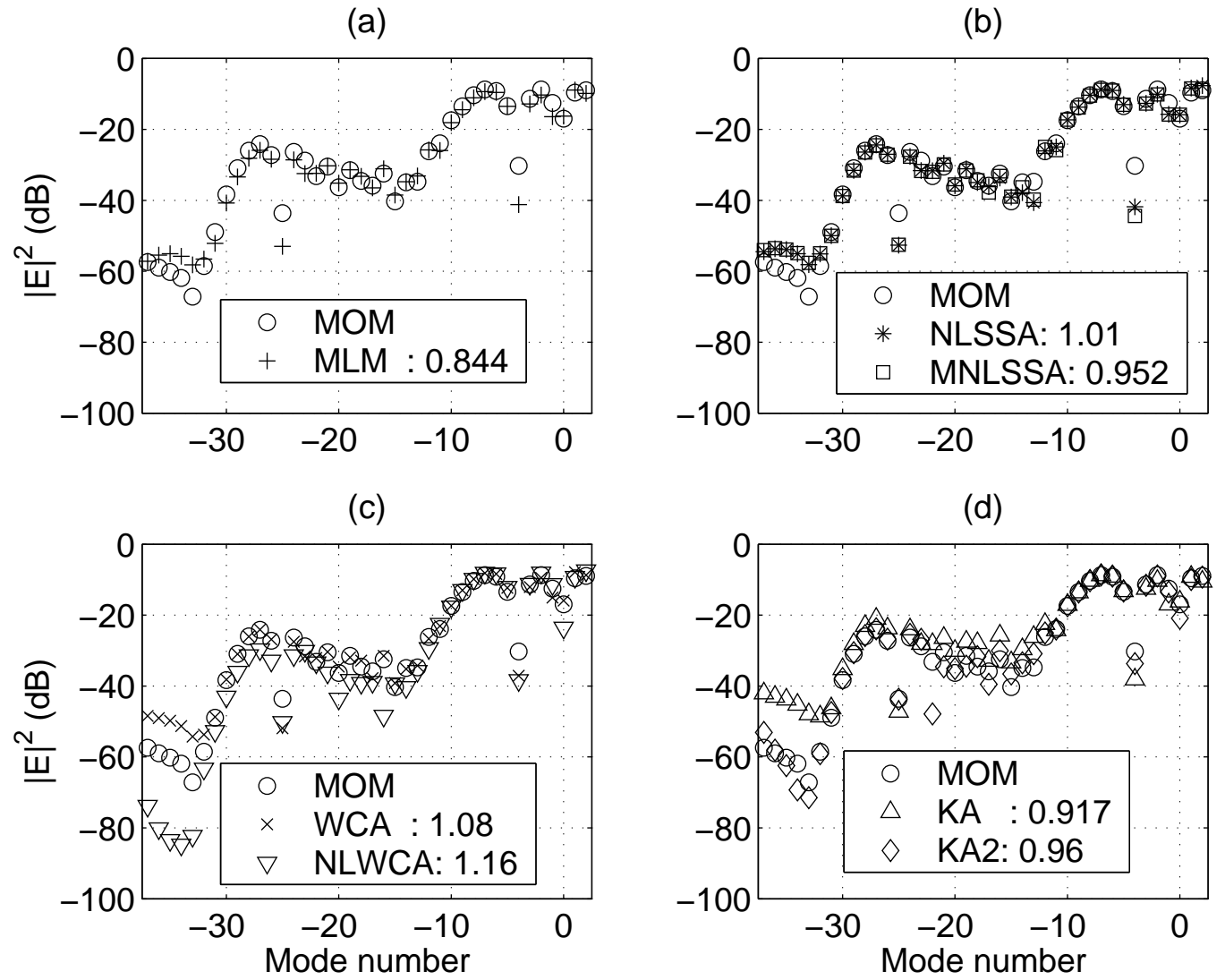


Figure 6. Comparison between rigorous and local approximate models for $A = \lambda$, $P = 20\lambda$, $A_2 = 0.03\lambda$, $P_2 = \lambda$, $\Phi = \pi/3$ (a) MoM and MLM (b) MOM, NLSSA, and MNLSSA (c) MOM, WCA-1, and WCA-1+NLWCA-2 (d) MOM, KA, and KA-2